Cell

Detection of Rare Antigen-Presenting Cells through T Cell-Intrinsic Meandering Motility, Mediated by Myo1g

Audrey Gérard,[1] Genaro Patino-Lopez,[2,4] Peter Beemiller,[1] Rajalakshmi Nambiar,[3] Khadija Ben-Aissa,[2] Yin Liu,[2] Fadi J. Totah,[1] Matthew J. Tyska,[3] Stephen Shaw,[2,5] and Matthew F. Krummel[1,*]
[1]Department of Pathology, University of California, San Francisco, 513 Parnassus Avenue, HSW512, San Francisco, CA 94143-0511, USA
[2]Experimental Immunology Branch National Cancer Institute, Bethesda, MD 20892-1360, USA
[3]Cell and Developmental Biology Department, Vanderbilt University School of Medicine, Nashville, TN 37205, USA
[4]Present address: Laboratorio de Investigación en Inmunología y Proteómica, Hospital Infantil de México, Federico Gómez, México City 06720, México
[5]Present address: NCI, NIH, Bethesda, MD 20892-1360, USA
*Correspondence: matthew.krummel@ucsf.edu
http://dx.doi.org/10.1016/j.cell.2014.05.044

SUMMARY

To mount an immune response, T lymphocytes must successfully search for foreign material bound to the surface of antigen-presenting cells. How T cells optimize their chances of encountering and responding to these antigens is unknown. T cell motility in tissues resembles a random or Levy walk and is regulated in part by external factors including chemokines and lymph-node topology, but motility parameters such as speed and propensity to turn may also be cell intrinsic. Here we found that the unconventional myosin 1g (Myo1g) motor generates membrane tension, enforces cell-intrinsic meandering search, and enhances T-DC interactions during lymph-node surveillance. Increased turning and meandering motility, as opposed to ballistic motility, is enhanced by Myo1g. Myo1g acts as a "turning motor" and generates a form of cellular "flânerie." Modeling and antigen challenges show that these intrinsically programmed elements of motility search are critical for the detection of rare cognate antigen-presenting cells.

INTRODUCTION

Search is a universal requirement in many biological systems: from a predator strategy to locate prey to the meandering search that T cells undertake to identify foreign peptides presented by major histocompatibility complex (MHC) molecules on antigen-presenting cells (APCs). This latter search has been described as having features of a Brownian random walk (Miller et al., 2003; Preston et al., 2006) or a Levy walk (Harris et al., 2012). The efficiency of this random-like motility pattern observed for T cells in lymph nodes (LNs) has been heavily modeled (Beauchemin et al., 2007; Beltman et al., 2009; Textor et al., 2011); however, perturbing cellular motility patterns in vivo has not previously been possible.

To optimize initial detection of antigens, a T cell must balance migration speed with the need to dwell in a given location for long enough to detect bona-fide signaling complexes and become activated. Furthermore, it must meander sufficiently to fully explore a region before departing to scan neighboring areas. The apparently random motility of T cells in tissues may arise through the combinations of three main mechanisms. First, the curved underlying stromal network of LNs may guide motility in convoluted patterns matching these structures (Bajénoff et al., 2006; Katakai et al., 2004). Second, the LN is seeded with micropatterns of highly localized and variable chemokine gradients (Bromley et al., 2008). Finally, it has been suggested that cell-intrinsic mechanisms would control T cell interstitial migration and contribute to tissue surveillance (Mrass et al., 2010), but direct evidence for this is lacking.

The intrinsic rate of T cell motility is determined by the rate of actin polymerization (Serrador et al., 1999; Vicente-Manzanares et al., 2002) coupled with the bundling actions of molecules such as crosslinked myosin IIA (Jacobelli et al., 2009). Motility under some (Overstreet et al., 2013) but not all (Friedl et al., 1998; Jacobelli et al., 2010; Woolf et al., 2007) 3D environments requires the coordinated activity of integrins, presumably to transmit sufficient force to pull nuclei through restrictive spaces or move against flow. Actin polymerization rate can be inhibited by tension of the cell membrane (Oster and Perelson, 1987). Cell-intrinsic control of directional persistence, the tendency not to turn, is less clear. Although chemokines again may function as guidance cues, T cells in 3D environments show an intrinsic propensity to "weave" (Jacobelli et al., 2010), a feature shared with many other amoeboid cells including neutrophils (Inoue and Meyer, 2008) and Dictyostelium (Andrew and Insall, 2007; Fukui, 2002). How this plays out in random search strategies such as those undertaken by T cells is yet to be examined.

Class I myosins are the largest group of unconventional myosins (Coluccio, 2008; Kim and Flavell, 2008). They are monomeric motor proteins that interact with actin filaments within cells

and, through lipid-binding C-terminal domains, associate with cellular membranes (Greenberg and Ostap, 2013; McConnell and Tyska, 2010). These associations generate membrane tension in at least one isoform, myosin 1a (Nambiar et al., 2009). Additionally, it has been suggested that these motors may act to sense forces on the membrane and actively oppose them (Laakso et al., 2008). How this family contributes to cellular motility remains largely undiscovered.

In this study, we identified myosin 1g (Myo1g) as a prominent class I myosin motor highly expressed in murine T cells. We found that Myo1g transiently accumulates in discrete areas at the plasma membrane of migrating cells or when membranes are deformed. Although T cells genetically deleted for Myo1g had global reduction in membrane tension, their homeostatic tissue distribution and responsiveness to T cell receptor (TCR) engagement were indistinguishable from wild-type (WT) cells. However, deficient cells moved faster and straighter. This combination of phenotypes allowed for side-by-side empirical and in silico modeling of the critical features of T cell search. Although Myo1g$^{-/-}$ cells covered territory more quickly due to increased velocities and straighter paths, this ultimately proved to be a deficit, specifically for detection of rare antigens. This highlights that random walk motility is tuned in part from within and generates optimal combinations of speed and local dwell time.

RESULTS

Myo1g is a hematopoietic specific myosin (Olety et al., 2010; Patino-Lopez et al., 2010) and the most heavily transcribed class I myosin in naive CD4 and CD8 T cells (Figure 1A). To understand the function of this class I myosin in T cells, we used targeted mutagenesis to generate mice lacking this motor protein (Figures S1A and S1B available online). Offspring were viable and healthy, and western blot confirmed the loss of Myo1g protein (Figure S1C). The cellularity and composition of thymus, spleens, and LNs from knockout (KO) animals were grossly normal (Figure S1D and data not shown).

Myosin I isoforms have a prominent role as force-sensitive motors, are located on cell membranes, and can regulate membrane tension (Gillespie and Cyr, 2004; Laakso et al., 2008; Nambiar et al., 2009). We performed tether force assays that demonstrated that Myo1g deficiency resulted in a dramatic reduction in the initial force required to pull membrane away from the cortex as well as a reduction in the force required to continue elongating a tether (Figures 1B and 1C). Consistent with a direct effect of Myo1g on membrane tension, a YFP-Myo1g fusion co-localized with the membrane marker DiD when T cells were plated onto integrin-coated glass substrates (2D) (Figures 1D and S1E), suggesting that Myo1g was anchored to the plasma membrane. However, when T cells were plated in complex 3D microchannels (Jacobelli et al., 2010), which mimic the spatial constraints experienced by T cells in vivo, we observed additional transient local accumulations (Figures 1E and 1F). Enrichment of YFP-Myo1g at the leading edge typically preceded motility arrest, and accumulation at side edges coincided with turns; in these cases, the portion of membrane in which Myo1g had accumulated would ultimately retract, and another portion of the leading edge dominated the direction of motility (Figure 1E).

The difference between Myo1g localization during 2D and 3D migration suggested that Myo1g accumulated in 3D in response to additional and/or asymmetric pressure generated through contacts within the 3D environment. Indeed, when we applied local pressure with a needle tip to cells migrating in a 2D environment, YFP-Myo1g was recruited to the site of pressure, often accompanied by accumulation of a membrane-targeted tdTomato (Figure 1G and Movie S1). The ratio between YFP-Myo1g and membrane fluorescence intensities was increased at the site of pressure application (Figures 1H and 1I), suggesting that Myo1g accumulation was not solely due to membrane accumulation. Consistent with this, transient accumulation during 3D migration required a functional motor domain of Myo1g (Figure S3B).

To test whether Myo1g controls T cell migration in a 3D environment, we used microchannels. These channels give control over confinement and adhesiveness (Jacobelli et al., 2010) while eliminating other external factors, allowing us to investigate a cell-intrinsic mode of T cell migration. We first analyzed T cell behavior in channels with relatively narrow widths that we have previously shown to optimize T cell speed (Jacobelli et al., 2010) (Figure 2A and Movie S2). When T cells migrated through an 8 μm-wide microchannel, two major behaviors could be observed, as cells alternated between migrating and arrested phases (Figure 2B). Typically, WT T cells would arrest for only short periods; 86% of WT T cells would either migrate continuously or stop for less than 20% of the time they were imaged and then resume migration (Figures 2A–2C). Whereas 10.5% of WT T cells were arrested for at least half of the time they were imaged, 53% of Myo1g$^{-/-}$ T cells did so (Figures 2A–2C). Interestingly, this stopping behavior was not apparent during 2D migration (not shown), reminiscent of the absence of Myo1g transient and local accumulation in 2D (Figures 1D and 1F), and suggesting that migration in 2D and 3D environments are differentially regulated. However, when motile, T cells from Myo1g$^{-/-}$ mice moved nearly twice as fast as T cells from WT mice (Figure 2D).

We noticed in microchannels containing more than one T cell that arrested cells were able to reinitiate migration when they encountered and were pushed by migrating cells (Movie S3, Figure 2E, and data not shown). In the absence of external force, we found that spontaneous reinitiation of migration was defective in Myo1g$^{-/-}$ T cells (Figure 2F). Consistent with this concept, we found that Myo1g deletion resulted in an increased percentage of cells with rounded morphology when in microchannels (Figure S2A). To test whether Myo1g facilitated reinitiation of polarization and symmetry breaking, we challenged cells to repolarize following wash-out of blebbistatin, a drug that acutely causes cells to round up (Movie S4). In this context, Myo1g$^{-/-}$ T cells required approximately three times as long to reinitiate polarization compared to their control counterparts (Figure 2G). Similar delay was observed when other chemicals, such as Nocodazole, were used to inhibit polarization (data not shown). Myo1g$^{-/-}$ T cells were ultimately able to polarize, as confirmed by localization of CD44 at the uropod and enrichment of phalloidin stain at the leading edge (Figure 2H). Finally, because Myo1g$^{-/-}$ T cells

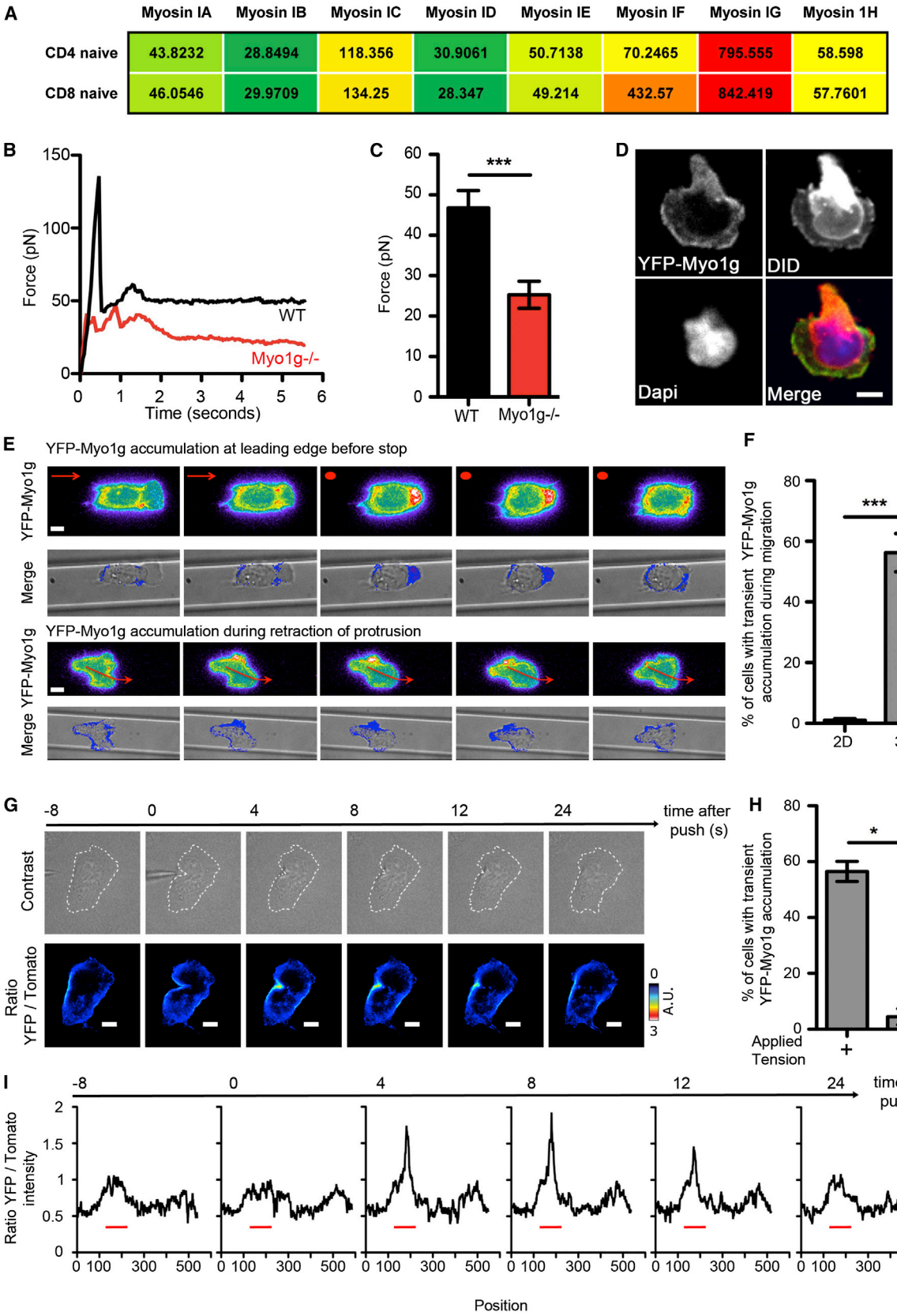

(legend on next page)

migrate faster, we also analyzed the function of Myo1g on the opposite transition, i.e., whether cells deficient in Myo1g would have a defect in transitioning from a polarized to a rounded morphology. We quantified in 2D (a condition in which we did not see any increased stopping due to Myo1g deficiency) whether Myo1g$^{-/-}$ cells would have the tendency to stay polarized longer, which should be reflected by the percentage of cells polarized at any time point, and did not find any difference in this measure (Figure S2B). Together, these data demonstrate that although these cells do not have a global defect in polarization, they are delayed in generating a leading edge from a rounded morphology. Such data are consistent with a requirement for asymmetric application of membrane tension in amoeboid motility (Houk et al., 2012).

Because we often observed Myo1g transiently accumulating along cell margins as a cell veers away from that space, we speculated that Myo1g might encourage T cell turning. We therefore quantified the frequency at which a given cell would change direction while migrating in thin microchannels. We found that Myo1g$^{-/-}$ cells underwent approximately three times fewer complete changes in direction (“u-turns”) (Figures 3A and 3B). In larger microchannels, activated T cells weave between opposing walls rather than crawling forward along a single wall (Jacobelli et al., 2010) (Figure 3C and Movie S5). The weaving angle as T cells turned away from each sidewall was significantly shallower for Myo1g$^{-/-}$ cells as compared to controls (41.3° ± 2° for WT and 29° ± 2° for Myo1g$^{-/-}$ and Figure 3D). We confirmed these results by analyzing T cell migration in 3D collagen matrices. Again, Myo1g deletion induced increased speed (Figure 3E), decreased turning angle (Figure 3F), but also increased rounded morphology (Figure S2C), herein demonstrating that T cells retain intrinsic migration features even when within a fiber network. Finally, we confirmed that decreased weaving angles of Myo1g$^{-/-}$ T cells as they turn were not solely due to increased speed (Figure S2D). Taken together, this analysis reveals a role for Myo1g in regulating intrinsic speed as well as the propensity to turn.

We then investigated whether Myo1g regulation of cell migration could be attributed to membrane tension. In a first set of experiments, we artificially increased membrane tensions in cells migrating in 2D environments by adding a hypotonic buffer that causes swelling and increased tension (Keren, 2011). This treatment reduced and therefore rescued cell speed of Myo1g$^{-/-}$ cells (Figure S3A). We noted that WT cells were also sensitive to hypotonic treatment, suggesting that additional tensioning systems may exist in T cells. In a second set of experiments, we tested whether a Myo1g mutant that was properly localized at the plasma membrane, but did not transiently accumulate during migration in 3D (Figures S3B and S3C), was able to rescue migration of Myo1g$^{-/-}$ cells. This motor-deficient mutant (IQ-Tail) could not link actin to the plasma membrane. Whereas full-length (FL) Myo1g restored T cell speed (Figure S3D) and T cell weaving angles (Figure S3E) of Myo1g$^{-/-}$ T cells migrating in microchannels to WT values, the mutant IQ-Tail did not. Altogether, we conclude that T cells have an intrinsic mode of migration regulated by Myo1g in a motor-dependent manner, most likely through global and discrete regulation of membrane tension.

Meandering by naive T cells in secondary lymph organs is not mechanistically well-understood (Germain et al., 2012; Mempel et al., 2004; Miller et al., 2003). To address whether Myo1g regulates random walk motility, WT and Myo1g$^{-/-}$ T cells were tracked in the T cell zone of LNs where they were found in the same intranodal space (Figure 4A, Movie S6, and data not shown). As we observed in vitro (Figure 3), motility tracks demonstrated a strong tendency for Myo1g$^{-/-}$ cells to move in straighter paths through the LN (Figures 4A and 4B). Quantification of their speed showed that they also moved approximately 50% faster on average (Figures 4A and 4C). Further track analysis showed that the average turning angle between 30 s frames was reduced from 52° for WT T cells to 40° for the Myo1g$^{-/-}$ T cells (Figure 4D). We never observed enhanced arrest in Myo1g$^{-/-}$ cells in LNs, presumably due to the multitude of mechanical pushing forces generated in this environment or due to local chemokine gradients.

Although our analysis of in vitro migration in simplified 3D environments demonstrated that Myo1g regulated an autonomous mode of cell migration (Figures 2 and 3), we verified that differences in migration patterns in vivo were not influenced by a defect in responding to external factors such as integrin ligands or chemokines. Myo1g$^{-/-}$ T cells expressed normal levels of

Figure 1. Myo1g Regulates Membrane Tension and Transiently Accumulates during T Cell Migration in 3D Environment or after Membrane Tension Perturbation

(A) Heatmap showing class I myosin gene expression in naive CD4 and CD8 T cells from LNs. Data are microarray data from the Immgen resource.

(B) Individual tether force records of WT (black) and Myo1g$^{-/-}$ (red) T cells.

(C) Average steady-state tether force measurements on WT (black) and Myo1g$^{-/-}$ (red) T cells (n = 5). ***p < 0.001.

(D–F) YFP-Myo1g-expressing OT-I cell blasts were harvested at days 4 to 5 after activation. (D) Snapshot showing representative YFP-Myo1g localization in cells migrating on ICAM-1-coated coverslips (“2D”). Upper left: YFP; upper right: membrane labeling DID; lower left: DAPI; lower right: merge. Scale bar represents 3 μm. (E) Images represent individual time points chosen from live-imaging time courses of YFP-Myo1g-expressing T cells migrating in ICAM-1-coated microchannels (“3D”). YFP-Myo1g fluorescence is shown in pseudocolor (YFP-Myo1g), or overlaid with bright-field images (merge). Scale bar represents 3 μm. Arrows indicate direction of migration, circles indicate a stopped cell. (F) Quantification of transient YFP-Myo1g accumulation in cell migrating in 2D versus 3D environment. Cell was scored positive if it displayed any localized increase in fluorescence intensity during the imaging period. Data correspond to two independent experiments. n > 50, ***p < 0.001.

(G–I) YFP-Myo1g-expressing T cell blasts generated from mTomato mice were allowed to migrate on ICAM-1-coated coverslip. Mechanical forces were applied by “pushing” the cell with a needle tip. Cells were imaged at 2–4 s intervals, using a 63× objective. (G) Snapshots showing representative YFP-Myo1g accumulation at the site where mechanical stress was applied. Upper panel: DIC; lower panel: ratio between YFP and Tomato fluorescence intensity is shown in pseudocolor. A.U.: arbitrary unit. Scale bar represents 3 μm. (H) Quantification of transient YFP-Myo1g local accumulation as in (F) before and after application of mechanical forces. Data correspond to four independent experiments. *p < 0.05, n = 32. (I) Graphs show the ratio between YFP and membrane (mTomato) fluorescence intensities along the cell surface at different times following application of membrane pressure. Site of pressure is depicted by a red line.

See also Figure S1.

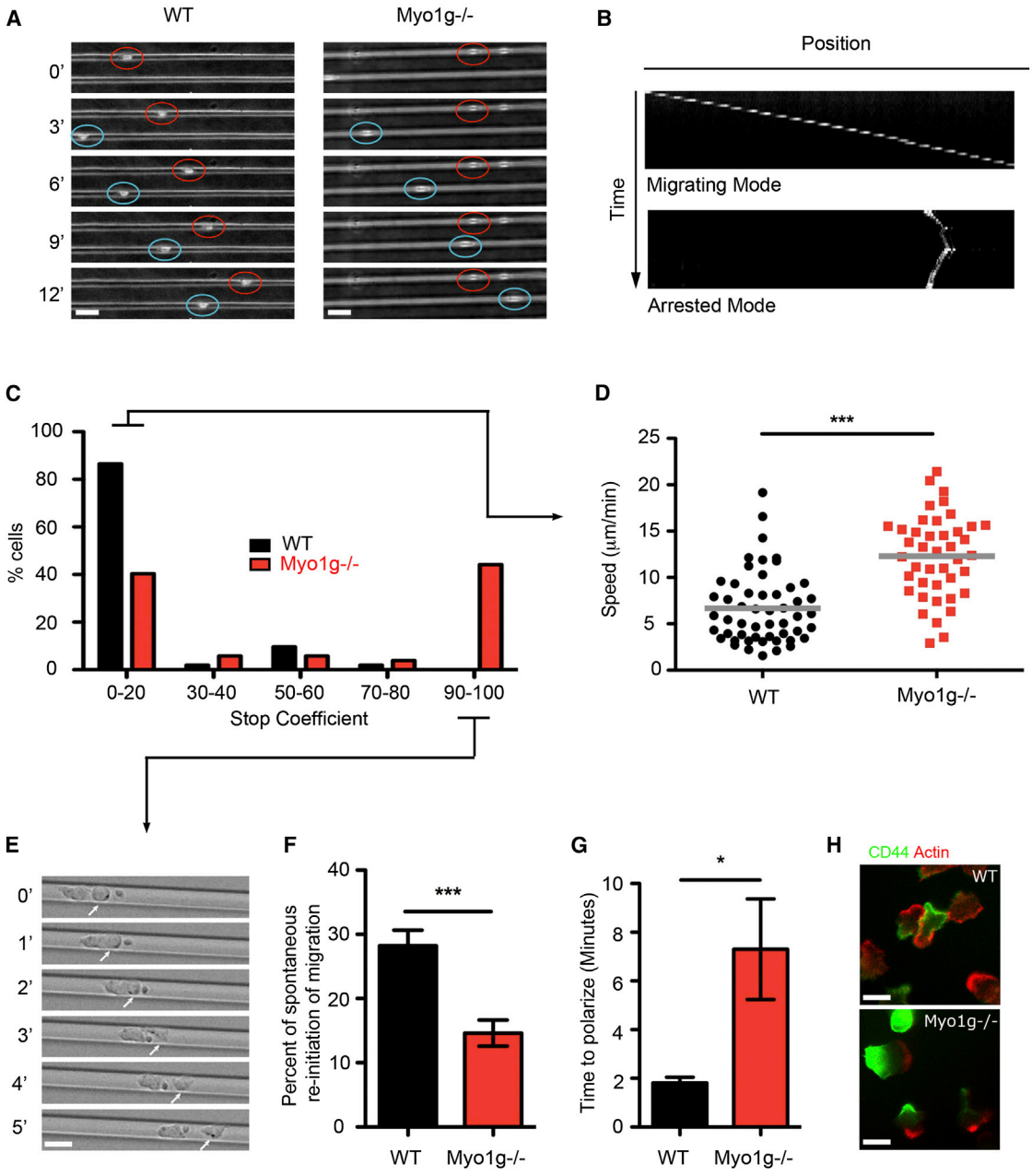

Figure 2. Myo1g Controls T Cell Speed and Reinitiation of Migration

(A–F) T cells isolated from WT or Myo1g$^{-/-}$ mice were introduced into ICAM-1-coated microchannels (A–D: 8 μm wide; E and F: 20 μm wide). (A) Bright-field images represent individual time points chosen from live-imaging time courses. Red and blue circles outline T cell positions; numbers indicate time in minutes. Scale bar represents 10 μm. (B) Kymograph-basis for analysis of T cell migration versus arrest. Kymographs are selected examples. (C) Graph shows the percentage of WT (black) and Myo1g$^{-/-}$ (red) cells stopping. The stop coefficient corresponds to percentage of time a cell was arrested over total time this cell was imaged. Data represent one representative experiment of two independent experiments (n = 50). (D) Graph shows mean velocities for WT (black) and Myo1g$^{-/-}$ (red) T cells under 3D confinement. Data correspond to three independent experiments. ***$p < 0.001$. (E) Snapshots showing a cell reinitiating polarization and migration when pushed by another migrating cell. Numbers represent time in minutes. Scale bar represents 10 μm. (F) Graph shows the percentage of arrested WT (black) or Myo1g$^{-/-}$ (red) cells that reinitiated migration without any external stimuli, compared to cells that were pushed by another cell (n = 62). Cells that did not move at all during the imaging period were excluded. Data correspond to three independent experiments. *$p < 0.05$.

(G and H) WT or Myo1g$^{-/-}$ naive T cells migrating on ICAM-1-coated coverslips were treated with blebbistatin for 10 min, and the inhibitor was washed away. (G) Graph shows the time necessary for the cells to reinitiate polarization (n = 120). Data correspond to three independent experiments. *$p < 0.05$. (H) Cells were fixed 20 min after washing the inhibitor and stained for CD44 and actin. Pictures are representative of two independent experiments. Scale bar represents 10 μm. See also Figure S2.

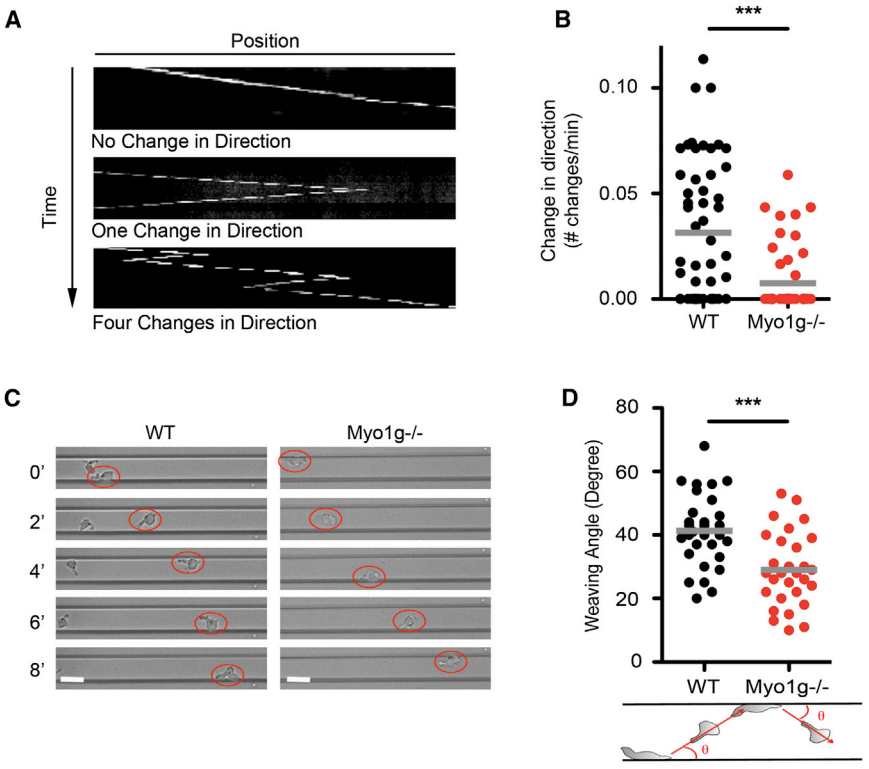

Figure 3. Myo1g Regulates Autonomous T Cell Weaving during Migration in 3D

(A–D) T cells isolated from WT or Myo1g$^{-/-}$ mice were introduced into ICAM-1-coated microchannels. (A) Kymograph-basis for analysis of change in direction in 8 μm-wide microchannels. Kymographs are selected examples. (B) Change in direction (number of times that a cell changed direction in 1 min) of WT (black) and Myo1g$^{-/-}$ (red) T cells migrating in 8 μm-wide microchannels. Data are from three independent experiments. ***$p < 0.001$. (C) Bright-field images of live-imaging time courses of cells migrating in 20 μm-wide microchannels. Red circles outline T cell positions during weaving; numbers indicate time in minutes. Scale bar represents 10 μm. (D) Mean weaving angle (angle a given cell bounces from one wall to the opposite wall) of WT (black) and Myo1g$^{-/-}$ (red) T cells migrating in 20 μm microchannels. Data are from three independent experiments. ***$p < 0.001$.

(E and F) T cells isolated from WT or Myo1g$^{-/-}$ mice were embedded and allowed to migrate in collagen lattices. Graphs show mean speed (E) and turning angle (F) of migrating WT (black) and Myo1g$^{-/-}$ (red) T cells. Data correspond to two independent experiments. ***$p < 0.001$.

See also Figure S3.

integrins LFA-1 and chemokine receptor CCR7 expression (data not shown), and they were as competent as their WT counterparts to adhere to integrin ligands (Figure 4E) and to respond to chemokines such as SDF1α (Figures 4F, S4A, and S4B). Normal overall response to tissue was also supported by the observation that B and T cell populations appear at normal frequencies (Figure 4G) and numbers (data not shown) in LNs of Myo1g$^{-/-}$ animals, and that homing to LNs was not impaired by Myo1g deficiency (data not shown).

Based on these data, Myo1g-deficient T cells were more "ballistic," i.e., they could cover territory faster as assessed by path length (Figure 5A) but simultaneously expanded the radius of their search (i.e., underwent displacement) at a faster rate (Figure 5B). Given that the ratio of these, loosely representing the degree of saturation of volumes actually surveyed versus potentially surveyed, was similar between WT and KO cells (Figure 5C), we hypothesized that their efficiency for running into relatively fixed targets might not be improved. We thus initially evaluated LN surveillance (*Search*) by modeling and quantifying the efficiency with which WT and Myo1g$^{-/-}$ T cell tracks, taken from live-imaging data in LNs, would intersect randomly placed in silico "APC targets" inside a sphere, placing the starting point of T cell tracks at the centroid (Figure 5D). Previous modeling showed that increased T cell speed (without altering turning patterns) increases LN surveillance (Beltman et al., 2007), but over hundreds of simulations, we found only subtle differences in the frequency with which 20–30 min tracks from WT and Myo1g$^{-/-}$ intersected in silico targets (Figures 5E and 5F). Similar effects were seen when path segments were assembled into artificial 12 hr tracks (Figures S4C–S4F), and these results concur with data on other biological search strategies in which ballistic motility is not necessarily more efficient (Reynolds and Bartumeus, 2009).

Reasoning that fewer turns and faster migration might regulate the dwell time for surveying targets (illustrated in Figure 5G), we also performed live-imaging of WT and Myo1g$^{-/-}$ T cells in excised LNs from mice that had been transferred with labeled activated DCs (without antigen) and quantified the time spent in contact for each T-DC encounter (which

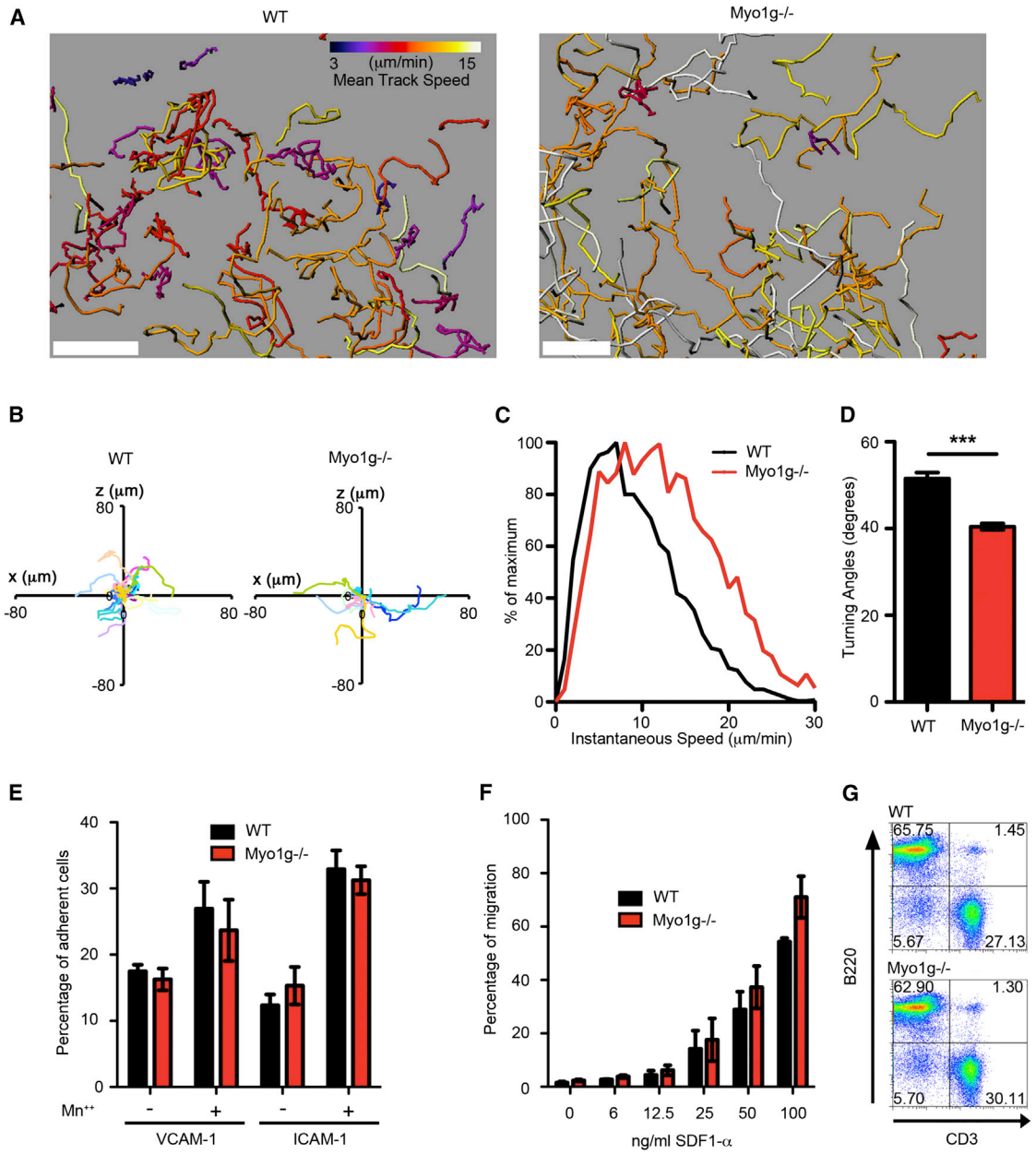

Figure 4. Myo1g Generates Meandering Interstitial Migration

(A–D) Migratory behavior of fluorescently labeled WT and Myo1g$^{-/-}$ OT-I cells inside WT LNs. (A) Image of a region of the T cell zone showing tracks for WT (left) and Myo1g$^{-/-}$ (right) T cells. Tracks are color-coded according to the mean track speed. Scale bar represents 50 μm. (B) Representative tracks in the xy plane of control T cells (left plot) and Myo1g$^{-/-}$ T cells (right plot) over a 15 min period. Starting coordinates are set to the origin. Units are in micrometers. Each colored line represents a single T cell track. (C) Instantaneous velocity profiles of WT (black) and Myo1g$^{-/-}$ (red) OT-I cells. Histograms show the relative frequency distribution of the two populations. (D) The median turning angle was calculated for each cell and plotted for each group (WT, black and Myo1g$^{-/-}$, red). Data are from three independent experiments. ***$p < 0.001$.

(E) Percentage (%) of WT (black) and Myo1g$^{-/-}$ (red) T cells that adhered to integrin-coated plates.

(F) WT (black) and Myo1g$^{-/-}$ (red) OT-I T cells were labeled with CFSE and CMTMR, respectively, mixed at a ratio 1:1 and subjected to a Boyden chamber assay. Percentage of cells that migrated toward the indicated dose of SDF1α was quantified by flow cytometry. The data are representative from three independent experiments.

(G) Flow cytometry analysis of T cell (CD3^{+}) and B Cell populations (B220^{+}) in LNs.

See also Figure S4.

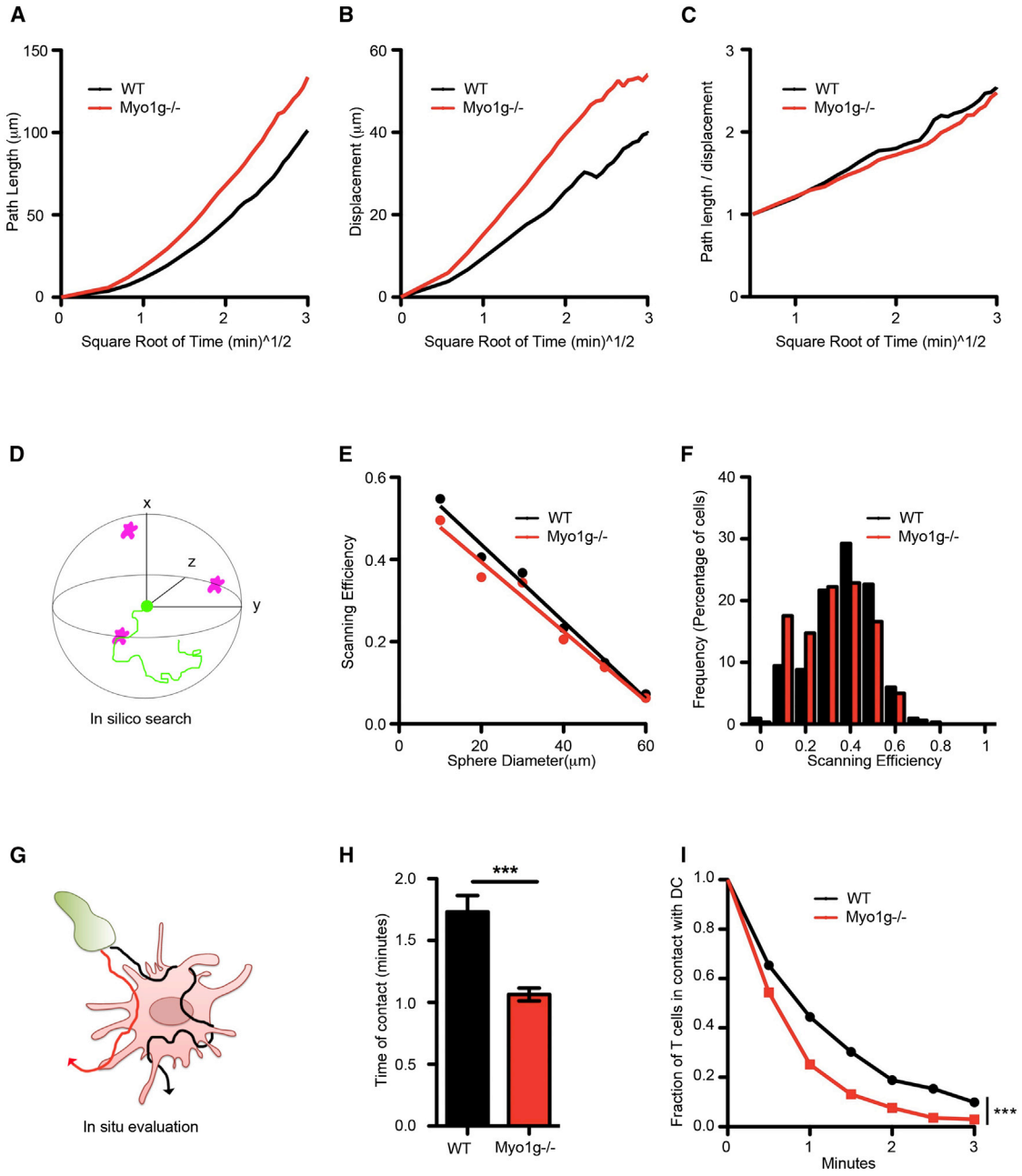

Figure 5. Defective LN Surveillance of Myo1g$^{-/-}$ T Cells

(A–C) Migratory behavior of fluorescently labeled WT and Myo1g$^{-/-}$ OT-I cells inside WT LNs. Representative experiment showing path length (A), mean displacement (B), and the ratio between path length and mean displacement (C) of WT (black) and Myo1g$^{-/-}$ (red) OT-I cells over square root of time.

(D–F) *Lymph node search*. (D) T cell tracks start at the origin of a sphere where targets are placed randomly. Track is scored positive if it crosses a target. (E) Scan efficiency (probability a track touches a target) relative to the diameter of the sphere. (F) Frequency of scan efficiency for a sphere diameter of 20 μm.

(G–I) *DC evaluation*. (G) The time a T cell (green) was in contact with a single DC (pink) was deduced from 2P data (see Experimental Procedures). Red and black lines illustrate trajectories of T cells. (H) Average time WT or Myo1g$^{-/-}$ T cells contact a DC. ***$p < 0.001$, $n = 50$. (I) Fraction of cells still in contact with a DC over time. ***$p < 0.001$, $n = 70$.

See also Figure S4.

we refer to as *Evaluation*). T cells deficient for Myo1g spent less time in contact with DCs (Figure 5H). Off-rate analysis showed that only 25% of Myo1g$^{-/-}$ T cells were in contact with a DC for at least 1 min, compared to 45% of control cells (Figures 5I and S4G). We conclude that migration patterns generated by Myo1g amplify the time a T cell scans

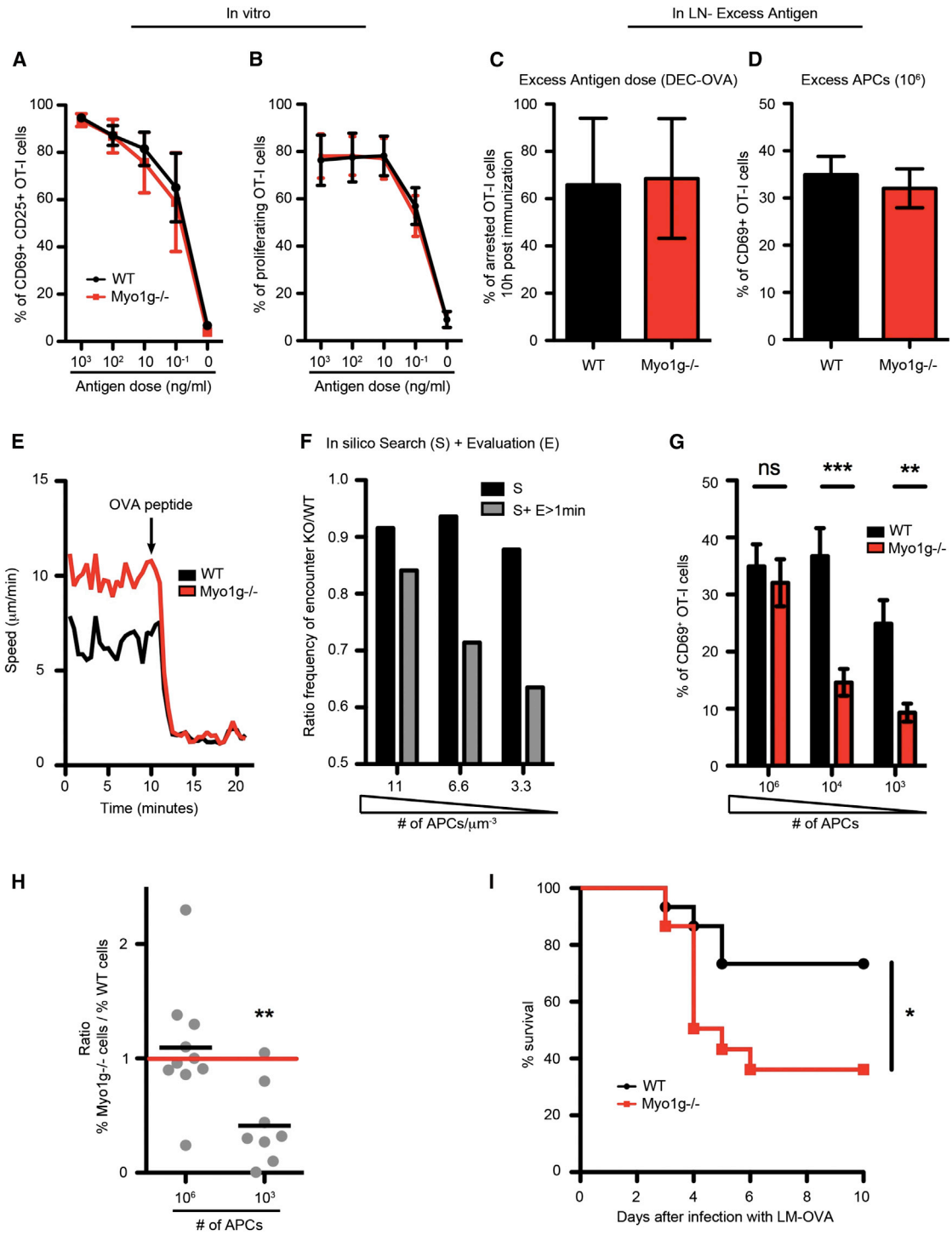

Figure 6. Cell-Intrinsic Migration Regulated by Myo1g Is Important for Immune Activation against Rare Antigens

(A and B) Percentage of WT (black) and Myo1g$^{-/-}$ (red) OT-I cells positive for CD25 and CD69 24 hr (A) or percentage of proliferating cells 72 hr (B) after activation in vitro with BMDCs pulsed with different doses of OVA peptide. Data are from three independent experiments.

(C and D) Mice bearing WT or Myo1g$^{-/-}$ OT-I cells were immunized with a high dose of antigen. (C) Mean arrest coefficient (percent of time a cell has a speed $\leq$ 2 μm/min) of WT (black) and Myo1g$^{-/-}$ (red) OT-I cells arrested in LN 8 hr after immunization with DEC-OVA. Data are from two independent experiments. (D) Percentage of OT-I cells positive for CD69 24 hr post-immunization with 10^6 OVA-pulsed APCs.

(E) Fluorescently labeled WT and Myo1g$^{-/-}$ OT-I cells were transferred in WT recipients, and LNs were explanted after 16 hr. Cells were imaged by two-photon microscopy for 10 min. OVA peptide was then added to the media perfusing the LN, and cells were imaged for another 10–15 min. Graph shows a representative

(legend continued on next page)

a DC while otherwise giving rise to similar efficiencies of "search."

What is the significance of Myo1g and this motility pattern for T cells? T cells specific for a particular antigen are rare in the naive repertoire (Blattman et al., 2002). Additionally, cellular repolarization and recognition of antigens on the surface of APCs lag ~1 min after initial contact (Krummel et al., 2000; Wülfing et al., 1997). Given that Myo1g deficiency reduced the time a T cell would evaluate a potential APC and that there was a 55% reduction in the percentage of T cells that were in contact with a DC for more than 1 min (Figure 5), we sought to take advantage of Myo1g$^{-/-}$ T cells to determine whether an autonomous mode of T cell migration optimized the efficiency of recognizing and responding to DCs.

We first established that TCR triggering by cognate antigen was not defective in Myo1g$^{-/-}$ T cells by the following criteria: (1) When WT and Myo1g$^{-/-}$ OT-I T cells, specific for an ovalbumin peptide, were challenged with antibodies against CD3 and CD28, they activated equivalently, as measured by upregulation of the activation marker CD69 or by proliferation (Figures S5A and S5B). (2) Activation (Figure 6A) and proliferation (Figure 6B) of these same cells in response to APCs pulsed with their cognate ovalbumin peptide were indistinguishable, even when using limiting concentrations of antigen. (3) Proximal calcium signaling was equivalent (data not shown). (4) Motility arrest and CD69 upregulation were equivalent between WT and Myo1g$^{-/-}$ OT-I cells when antigens were presented on a large population of APCs in vivo (Figures 6C and 6D). (5) Symmetry breaking necessary for synapse formation during antigen recognition was not impaired in vitro, as accessed by TCR microcluster dynamics (Figures S5C and S5D and Movie S7). (6) The rate of symmetry breaking during antigen recognition was also not impaired in vivo, as WT and Myo1g$^{-/-}$ T cells slowed their speed, stopped, and rounded up at the same rate following Ag recognition (Figure 6E and Movie S8). Thus, Myo1g deletion did not alter antigen recognition per se.

We then performed in silico efficiency modeling based on tracks from Figure 5 including a factor that takes into account an *Evaluation* or requisite mean detection time (Campos et al., 2013) for a T cell to find and respond to displayed peptide MHC (pMHC) on the APC. As expected, Myo1g tracks were comparatively less efficient when the model required T cells to undertake an evaluation period that was equal or greater (data not shown) to the observed ~1 min lag time for T cells to signal in response to APC contact (Figure 6F) (Krummel et al., 2000; Wülfing et al., 1997). In predator-prey searches, larger numbers of prey can compensate for poor detection. In this case, for minimal interaction times equal to or greater than the measured lag time (1 min), the decreased antigen detection efficiency of Myo1g$^{-/-}$ T cells is predicted to be rescued by increasing target density.

Based on these predictions, we determined whether Myo1g was required, empirically, for T cells to find and respond to rare APCs. WT or Myo1g$^{-/-}$ OT-I cells were transferred into mice, followed by immunization with graded numbers of APCs. One day after immunization, when transferred DCs had reached the LN (Figure S5E), equivalent fractions of WT and Myo1g$^{-/-}$ OT-I cells were activated when immunizing with a high number of DCs (Figure 6G). In contrast, the fraction of Myo1g$^{-/-}$ OT-I cells that were successfully triggered when a low number of APCs was transferred was decreased by 62% compared to WT OT-I cells (Figure 6G). This effect perpetuated out into the generation of clonal expansion; Myo1g$^{-/-}$ OT-I T cells had expanded to the same extent as WT counterparts when a large number of APCs was introduced (Figure 6H—10^6 APCs), but when APCs were rarer, Myo1g$^{-/-}$ OT-I T cells showed a 59% reduction in numbers compared to controls (Figure 6H—10^3 APCs). Finally, we examined whether search behavior regulated by Myo1g and optimized for discovering rare APCs was actually required for an adaptive immune response to infection. Mice bearing a physiological number of WT or Myo1g$^{-/-}$ OT-I cells were infected with a dose of *Listeria monocytogenes* expressing OVA, below the lethal dose $(LD)_{50}$. Whereas 75% of mice bearing control OT-I survived after challenge, only 35% of mice transferred with OT-I deficient in Myo1g did so (Figure 6I). We thus concluded that Myo1g and the motility patterns it imparts, though dispensable for antigen recognition per se, are nevertheless important for efficient surveillance.

DISCUSSION

In this study, we provide direct genetic evidence that turning in T cells is in part "hard-wired" and that a membrane-bound myosin 1 isoform supplies much of the basis for this behavior. Myo1g$^{-/-}$ T cells, which showed altered migration patterns in vitro and in vivo, are less efficient in scanning and evaluating APCs. Motility pattern, therefore, is a critical determinant of immune sensitivity to foreign antigens.

Myo1g is localized at the plasma membrane and displays transient accumulation during migration in 3D. Although significantly more biophysical data will be required to determine whether Myo1g is recruited by other molecules to membranes or is ubiquitous and autonomously force-sensing, our data clearly show that Myo1g is the source of a significant amount of the tension on the T cell membrane. Differential dynamic localization of Myo1g in T cells migrating in 2D or 3D also suggests that Myo1g

example (out of three independent experiments) of WT (black) and Myo1g$^{-/-}$ (red) cell speed over time (n > 50 for each cell type). OVA peptide addition is depicted by an arrow.

(F) LN search was assessed as in Figures 5D–5F. Graph shows the ratio of the frequency of encounter of KO tracks over WT tracks relative to target density. The efficiency of the search was calculated including or not an evaluation > 1 min.

(G and H) Mice bearing WT or Myo1g$^{-/-}$ OT-I cells were immunized with the indicated number of OVA-pulsed BMDCs (APCs). Percentage of OT-I cells positive for CD69 24 hr post-immunization (G) or ratio between the percentage of Myo1g$^{-/-}$ cells and percentage of WT cells 6 days post-immunization (H) are shown. Data are from four independent experiments. **p < 0.01 and ***p < 0.001.

(I) Mice (n = 10) were transferred with 5 × 10^3 WT (black) or Myo1g$^{-/-}$ (red) OT-I cells and were challenged with a sublethal dose of LM-OVA (0.25 × LD_{50}). Graph shows mouse survival over time.

See also Figure S5.

is particularly important in 3D. This follows on other emerging data that 2D and 3D motility have significantly different requirements and modes (Friedl et al., 2012). We hypothesize that global membrane tension, regulated, at least in part, by Myo1g, attenuates T cell speed, whereas localized changes in membrane tension by Myo1g are involved in T cell turning. Consistent with this, Myo1g$^{-/-}$ T cells migrating in a uniform soft media (2D) have increased speed compared to WT cells but equivalent path straightness (data not shown).

Myo1g function is likely complemented by other proteins such as those modulating the site of actin polymerization (Dang et al., 2013). The identity, role, and relationship to Myo1g of such other molecules will need to be elucidated. Modulation of tension at different sites and times also leads to apparent opposite phenotypes. For instance, deletion of Myo IIA in Dictyostelium induces a loss of cortical tension (as opposed to membrane tension), which is correlated with decreased cell speed (Jay et al., 1995), and in T cells, loss of myosin II leads to over-adherence and slow motility in vivo (Jacobelli et al., 2010). Establishing exact localization during migration and binding partners of those regulators is probably, here again, the key to our understanding of how tension within different regions orchestrates cell migration.

TCR triggering by T cells lacking Myo1g is unaffected in a multitude of assays, except when T cells are exposed to very low numbers of APCs. Infections with virus may generate far fewer than 100 APCs per LN (Usherwood et al., 1999), and early protective response to viruses limit both dissemination and ensuing destruction. Levels of cognate APCs in many immunizations and infection models are in the higher range of our assay and thus are likely oversaturating by the measures we have used.

Search is a feature of many biological systems, and it is well understood that ballistic modes of predatory searching, as by some sea birds, produce a search that is significantly incomplete (Miramontes et al., 2012). The phenotype of Myo1g$^{-/-}$ T cells and the modeling of their ''Search'' versus ''Evaluation'' dynamics provide an enlarged framework for additional understanding of immune search and surveillance. This work would suggest that future modeling will profit from including a parameter equivalent to the pre-exponential (or frequency) factor from chemical kinetics (Zhdanov et al., 1988). That factor ''k'' partially encompasses the likelihood that two or more chemical reactants bump into each other in a favorable orientation to facilitate the generation of products. In the case of T cell search, our study suggests that an optimum exists between high T cell speed (to increase the chance a T cell comes across a target) and the slower process of meandering (which puts the length of T-DC contacts in a range consistent with generation of signaling).

Cell motility in vivo is undoubtedly influenced by features of the LN itself, like the fibroblastic reticular cell (FRC) network and local chemotaxis. Our results do not necessarily negate the potential role of FRC in guiding motility. Because the FRC network of LNs is highly convoluted (Bajénoff et al., 2006; Katakai et al., 2004), straighter paths by Myo1g$^{-/-}$ cells compared to WT cells in the same region might still represent cells that are loosely attached and ''guided'' by these fibers but that take more straight choices at each FRC junction. In comparison to our findings, computational analysis suggests that the guidance afforded by the FRC network has only a minor effect on the probability to find rare APCs (Graw and Regoes, 2012).

Because Myo1g is not required for chemotaxis, the straighter paths taken by Myo1g$^{-/-}$ cells may imply that chemokines are not a prominent part of directional guidance cues for early antigen searches in the T cell zone. That situation likely changes when T cells get some degree of initial triggering and upregulate chemokine receptors such as CCR5 (Castellino et al., 2006; Hugues et al., 2007) or CXCR3 (Hu et al., 2011); cells that upregulate these in response to successful detection of an initial pMHC encounter may thereby be subsequently guided rather than relying on unguided search. Thus, the search that may matter in the case of rare-antigen detection relates to the ability of a T cell to find and successfully respond to its very first pMHC-bearing APC and to subsequently reach a threshold of engagement(s) for chemokine receptor expression. Beyond that, the chemokines generated by other successful clones may help a T cell to find additional APCs or cells already identified by clones responding in parallel.

This work exemplifies an unappreciated role for an unconventional class I myosin in the cell biology of motility. In mice and humans, class I myosins can be subdivided into short-tailed forms (Myo1a, b, c, d, g, and h) and long-tailed (amoeboid) forms (Myo1e and f). Of these, the long form Myo1f and the short forms Myo1c and Myo1g are enriched in lymphocytes (Patino-Lopez et al., 2010). Long-form Myo1f has been implicated in neutrophil adhesion (Kim et al., 2006), but in its case, this is likely due to its association with vesicular membranes leading to changes in integrin function. The loss of Myo1g did not affect integrin adhesion in T cells, suggesting that the specificity of the tail domain likely determines the relevant function for the particular myosin. Myo1c is strongly expressed in B cells, in which it participates in cytoskeleton rearrangements and antigen presentation (Maravillas-Montero et al., 2011).

To conclude, we provide evidence that Myo1g is a master regulator of membrane tension in T cells and is required for optimal meandering and successful LN surveillance.

EXPERIMENTAL PROCEDURES

Local Application of Pressure

Activated T cells generated from WT or mTomato mice were transduced with YFP-Myo1g. ICAM-1-coated chambers were obtained by coating 8-well chambers (Lab-Tek) with 5 μg/ml ICAM-1-Fc (R&D systems) in PBS for 1 hr at 37°C. Four to eight days after activation, cells were allowed to migrate on ICAM-1-coated coverslips for at least 2 hr. Mechanical stress was locally applied by using a glass probe with an inside diameter of 0.5 mm. Most cells demonstrated continual viability after pushing, and any cell that appeared damaged was not scored in this analysis. T cells were imaged for 2 min at intervals of 2–4'' with a modified microscope (Axiovert 200M; Carl Zeiss, Inc.) with Plan-Neofluar 63× objective (Carl Zeiss, Inc.).

Microchannel Fabrication and Imaging

Microchannel fluidic devices were fabricated, and cells were loaded in microchannels as already described (see Extended Experimental Procedures) (Faure-André et al., 2008; Jacobelli et al., 2010). T cells crawling in the microchannels were imaged for 60 min at intervals of 1 min. Metamorph software (Molecular Devices) was used for calculation of cell speed and directionality. For analysis of the localization of YFP-Myo1g constructs in migrating T cells, cells were imaged for 5 min at 5 s intervals. Images were acquired with an inverted Zeiss with Yokogawa CSU-10 Spinning

Disk. The imaging and control software used was MetaMorph (MDS Analytical Technologies). A minimum of 30 cells per microchannel width per treatment condition were analyzed.

Reinitiation of Polarization and Polarization Quantification

Coverslips were coated with 5 μg/ml ICAM-1 in PBS for 1 hr at 37°C. T cell blasts generated from WT or Myo1g$^{-/-}$ mice were allowed to migrate on ICAM-1-coated coverslips. Cells were treated with blebbistatin (racemic mix, 100 μM of the racemate, Calbiochem) for 10 min, and the inhibitor was washed away. T cells were imaged for 20 min at intervals of 10 s with a modified microscope (Axiovert 200M; Carl Zeiss, Inc.) with Plan-Neofluar 20× objective (Carl Zeiss, Inc.). For quantification of cell polarization, cells migrating on ICAM-1 coverslip (or alternately 20 min after washing blebbistatin away) were fixed in PBS 1% PFA 15 min at room temperature (RT) and permeabilized with 0.05% Saponin for 5 min at RT. Cells were stained with CD44-FITC and Phalloidin-Alexa 555 in PBS 2% BSA for 20 min at RT.

Two-Photon Imaging of Explanted Lymph Nodes

WT and Myo1g$^{-/-}$ OT-I cells were labeled with 2 μM CFSE and 20 μM CMTMR, respectively and ad-mixed, and 3 × 10^6 total cells were transferred to WT recipient. Switching dyes did not affect results (data not shown).

For DC Scanning Experiments

1 × 10^6 LPS-activated bone marrow-derived dendritic cells (BMDCs) from Act-CFP mice were injected subcutaneously in the footpad or the flank at the same time of T cell transfer.

For Analysis of Cells during the Arrest Phase

Mice were immunized subcutaneously in the footpad or the flank with 2 μg anti-DEC205 conjugates that were produced in house (Bonifaz et al., 2002; Gérard et al., 2013) together with 10 μg anti-CD40 (Clone 1C10, eBiosciences).

Popliteal, Inguinal, and Axillary LNs were taken out 16 to 24 hr after T cell transfer, or 8 hr after DEC-OVA immunization, and immobilized on coverslips with the hilum facing away from the objective. Time-lapse imaging was performed with a custom resonant-scanning instrument containing a four-photomultiplier tube (Hamamatsu) operating at video rate, as described (Friedman et al., 2010). Each xy plane spanned 288 μm × 240 μm at a resolution of 0.60 μm per pixel. Images of up to 35 xy planes with 3 μm z spacing were acquired every 30 s for 30 min.

Imaris (Bitplane) and Matlab software (Mathworks) were used to quantify T cell migration behavior. To characterize contact parameters between T cells and DCs, tracks and surface of T cells and DCs were generated, and the dwell time of interaction between surfaces was analyzed as previously described (Gérard et al., 2013): T cell–DC cell interaction was defined as the close association of a given OT-I cell surface with a DC surface for at least 1 min. A threshold of 4 μm between cell edges was used, which accounts for low fluorescence frequently encountered at cell edges, which fit manual quantification (data not shown).

Track Simulation

To overcome deficiencies in cell-based track analyses (Beltman et al., 2009; Textor et al., 2011), long duration tracks were simulated from shorter duration T cell tracks. Trajectories generated by tracking T cells that transited in LNs in the absence of antigen were pooled into control and Myo1g$^{-/-}$ cell groups. The instantaneous displacements (the x, y, and z displacements measured for each 30 s sampling interval) were calculated from all tracks in the two groups. Simulated tracks for WT and Myo1g$^{-/-}$ cells were then generated by randomly sampling the instantaneous displacements and cumulatively summing the selected displacements. One hundred and twenty-eight control and KO tracks lasting 12 hr were simulated.

Track Encounter Efficiency or Search Efficiency

To estimate the efficiency with which T cell tracks encountered a stationary dendritic cell, hypothetical target dendritic cells were placed in space at an average distance d from the T cell tracks' common origin. The distance d, in the range of 5–60 μm (experimental data) or 50–600 μm (simulated tracks), was supplied as an input parameter to the simulation. Dendritic cell positions were generated by sampling from a random uniform distribution with a mean of 2d, which placed the target dendritic cells, on average, d μm from the T cell tracks' origin. The distance for each target was combined with two random angles on the interval [0, 2π] to generate a spherical coordinate for each dendritic cell. A capture distance, defined as the sum of the dendritic cell radius and the T cell radius, was used to determine whether the T cell encountered a hypothetical dendritic cell. The dendritic cell radius (10 μm) was specified as an input parameter to the simulation, whereas the T cell radius was a randomly chosen value from the list of T cell radii measured as part of the in vivo tracking analysis. A T cell was considered to encounter a dendritic cell if at any point in the track, the distance between the T cell and dendritic cell positions was less than the capture distance. The simulation was repeated for 50 trials, with new dendritic cell positions generated for each trial.

Dwell Duration or Evaluation

To estimate the amount of time that T cells spent near dendritic cells in the absence of antigen, the track encounter efficiency simulation was modified to calculate the number of successive simulation frames that a T cell remained within the capture distance of a dendritic cell for each encounter. The distribution of the dwell durations was calculated, with a single-frame encounter assumed to represent a 30 s dwell time, a two-frame encounter assumed to represent a 60 s dwell time, etc.

Statistical Analysis

Data were expressed as mean ± SEM, unless specified. Comparisons between groups were analyzed with the t test or one-way or two-way Anova test, using GraphPad Prism software.

SUPPLEMENTAL INFORMATION

Supplemental Information includes Extended Experimental Procedures, five figures, and eight movies and can be found with this article online at http://dx.doi.org/10.1016/j.cell.2014.05.044.

AUTHOR CONTRIBUTIONS

A.G. designed and performed the experiments unless specified. G.P.-L. generated and characterized the thymic and peripheral populations in Myo1g$^{-/-}$ mice, performed adhesion assay, and together with A.G. made initial observation of increased migration speed of Myo1g$^{-/-}$ cells in vitro. F.J.T. assisted with cSMAC assays. Y.L. and K.B.-A. participated in Myo1g$^{-/-}$ mice characterization, and P.B. wrote MATLAB scripts for extrapolating T cell tracks and quantifying search and evaluation efficiency. S.S. conceived and participated in design and interpretation of some experiments, and M.F.K. conceived and participated in design and interpretation of all experiments. R.N. and M.J.T. performed analyses of membrane tension; A.G. and M.F.K. wrote, revised, and edited the manuscript.

ACKNOWLEDGMENTS

We thank the Biological Imaging Development Center personnel for technical assistance with imaging. We thank G.A. Bizarri, F. Bartumeus, G. Altan-Bonnet, D. Barber D. Erle, and S. Dumont for helpful comments and suggestions and the ImmGen consortium for array data. We thank M.B. Headley for critical reading of the manuscript. This work was supported by grants from NIH (DK075555) and American Heart Association to M.J.T., The NIH Intramural Research Program to S.S., and NIH (AI052116) to M.F.K.

Received: December 15, 2013
Revised: April 15, 2014
Accepted: May 20, 2014
Published: July 31, 2014

REFERENCES

Andrew, N., and Insall, R.H. (2007). Chemotaxis in shallow gradients is mediated independently of PtdIns 3-kinase by biased choices between random protrusions. Nat. Cell Biol. *9*, 193–200.

Bajénoff, M., Egen, J.G., Koo, L.Y., Laugier, J.P., Brau, F., Glaichenhaus, N., and Germain, R.N. (2006). Stromal cell networks regulate lymphocyte entry, migration, and territoriality in lymph nodes. Immunity *25*, 989–1001.

Beauchemin, C., Dixit, N.M., and Perelson, A.S. (2007). Characterizing T cell movement within lymph nodes in the absence of antigen. J. Immunol. *178*, 5505–5512.

Beltman, J.B., Marée, A.F., Lynch, J.N., Miller, M.J., and de Boer, R.J. (2007). Lymph node topology dictates T cell migration behavior. J. Exp. Med. *204*, 771–780.

Beltman, J.B., Henrickson, S.E., von Andrian, U.H., de Boer, R.J., and Marée, A.F. (2009). Towards estimating the true duration of dendritic cell interactions with T cells. J. Immunol. Methods *347*, 54–69.

Blattman, J.N., Antia, R., Sourdive, D.J., Wang, X., Kaech, S.M., Murali-Krishna, K., Altman, J.D., and Ahmed, R. (2002). Estimating the precursor frequency of naive antigen-specific CD8 T cells. J. Exp. Med. *195*, 657–664.

Bonifaz, L., Bonnyay, D., Mahnke, K., Rivera, M., Nussenzweig, M.C., and Steinman, R.M. (2002). Efficient targeting of protein antigen to the dendritic cell receptor DEC-205 in the steady state leads to antigen presentation on major histocompatibility complex class I products and peripheral CD8+ T cell tolerance. J. Exp. Med. *196*, 1627–1638.

Bromley, S.K., Mempel, T.R., and Luster, A.D. (2008). Orchestrating the orchestrators: chemokines in control of T cell traffic. Nat. Immunol. *9*, 970–980.

Campos, D., Bartumeus, F., and Méndez, V. (2013). Search times with arbitrary detection constraints. Phys. Rev. E Stat. Nonlin. Soft Matter Phys. *88*, 022101.

Castellino, F., Huang, A.Y., Altan-Bonnet, G., Stoll, S., Scheinecker, C., and Germain, R.N. (2006). Chemokines enhance immunity by guiding naive CD8+ T cells to sites of CD4+ T cell-dendritic cell interaction. Nature *440*, 890–895.

Coluccio, L.M. (2008). Myosin I. In Myosins: A Superfamily of Molecular Motors, L.M. Coluccio, ed. (The Netherlands: Springer).

Dang, I., Gorelik, R., Sousa-Blin, C., Derivery, E., Guérin, C., Linkner, J., Nemethova, M., Dumortier, J.G., Giger, F.A., Chipysheva, T.A., et al. (2013). Inhibitory signalling to the Arp2/3 complex steers cell migration. Nature *503*, 281–284.

Faure-André, G., Vargas, P., Yuseff, M.I., Heuzé, M., Diaz, J., Lankar, D., Steri, V., Manry, J., Hugues, S., Vascotto, F., et al. (2008). Regulation of dendritic cell migration by CD74, the MHC class II-associated invariant chain. Science *322*, 1705–1710.

Friedl, P., Entschladen, F., Conrad, C., Niggemann, B., and Zänker, K.S. (1998). CD4+ T lymphocytes migrating in three-dimensional collagen lattices lack focal adhesions and utilize beta1 integrin-independent strategies for polarization, interaction with collagen fibers and locomotion. Eur. J. Immunol. *28*, 2331–2343.

Friedl, P., Sahai, E., Weiss, S., and Yamada, K.M. (2012). New dimensions in cell migration. Nat. Rev. Mol. Cell Biol. *13*, 743–747.

Friedman, R.S., Beemiller, P., Sorensen, C.M., Jacobelli, J., and Krummel, M.F. (2010). Real-time analysis of T cell receptors in naive cells in vitro and in vivo reveals flexibility in synapse and signaling dynamics. J. Exp. Med. *207*, 2733–2749.

Fukui, Y. (2002). Mechanistics of amoeboid locomotion: signal to forces. Cell Biol. Int. *26*, 933–944.

Gérard, A., Khan, O., Beemiller, P., Oswald, E., Hu, J., Matloubian, M., and Krummel, M.F. (2013). Secondary T cell-T cell synaptic interactions drive the differentiation of protective CD8+ T cells. Nat. Immunol. *14*, 356–363.

Germain, R.N., Robey, E.A., and Cahalan, M.D. (2012). A decade of imaging cellular motility and interaction dynamics in the immune system. Science *336*, 1676–1681.

Gillespie, P.G., and Cyr, J.L. (2004). Myosin-1c, the hair cell's adaptation motor. Annu. Rev. Physiol. *66*, 521–545.

Graw, F., and Regoes, R.R. (2012). Influence of the fibroblastic reticular network on cell-cell interactions in lymphoid organs. PLoS Comput. Biol. *8*, e1002436.

Greenberg, M.J., and Ostap, E.M. (2013). Regulation and control of myosin-I by the motor and light chain-binding domains. Trends Cell Biol. *23*, 81–89.

Harris, T.H., Banigan, E.J., Christian, D.A., Konradt, C., Tait Wojno, E.D., Norose, K., Wilson, E.H., John, B., Weninger, W., Luster, A.D., et al. (2012). Generalized Lévy walks and the role of chemokines in migration of effector CD8+ T cells. Nature *486*, 545–548.

Houk, A.R., Jilkine, A., Mejean, C.O., Boltyanskiy, R., Dufresne, E.R., Angenent, S.B., Altschuler, S.J., Wu, L.F., and Weiner, O.D. (2012). Membrane tension maintains cell polarity by confining signals to the leading edge during neutrophil migration. Cell *148*, 175–188.

Hu, J.K., Kagari, T., Clingan, J.M., and Matloubian, M. (2011). Expression of chemokine receptor CXCR3 on T cells affects the balance between effector and memory CD8 T-cell generation. Proc. Natl. Acad. Sci. USA *108*, E118–E127.

Hugues, S., Scholer, A., Boissonnas, A., Nussbaum, A., Combadière, C., Amigorena, S., and Fetler, L. (2007). Dynamic imaging of chemokine-dependent CD8+ T cell help for CD8+ T cell responses. Nat. Immunol. *8*, 921–930.

Inoue, T., and Meyer, T. (2008). Synthetic activation of endogenous PI3K and Rac identifies an AND-gate switch for cell polarization and migration. PLoS ONE *3*, e3068.

Jacobelli, J., Bennett, F.C., Pandurangi, P., Tooley, A.J., and Krummel, M.F. (2009). Myosin-IIA and ICAM-1 regulate the interchange between two distinct modes of T cell migration. J. Immunol. *182*, 2041–2050.

Jacobelli, J., Friedman, R.S., Conti, M.A., Lennon-Dumenil, A.M., Piel, M., Sorensen, C.M., Adelstein, R.S., and Krummel, M.F. (2010). Confinement-optimized three-dimensional T cell amoeboid motility is modulated via myosin IIA-regulated adhesions. Nat. Immunol. *11*, 953–961.

Jay, P.Y., Pham, P.A., Wong, S.A., and Elson, E.L. (1995). A mechanical function of myosin II in cell motility. J. Cell Sci. *108*, 387–393.

Katakai, T., Hara, T., Lee, J.H., Gonda, H., Sugai, M., and Shimizu, A. (2004). A novel reticular stromal structure in lymph node cortex: an immuno-platform for interactions among dendritic cells, T cells and B cells. Int. Immunol. *16*, 1133–1142.

Keren, K. (2011). Cell motility: the integrating role of the plasma membrane. Eur. Biophys. J. *40*, 1013–1027.

Kim, S.V., and Flavell, R.A. (2008). Myosin I: from yeast to human. Cell. Mol. Life Sci. *65*, 2128–2137.

Kim, S.V., Mehal, W.Z., Dong, X., Heinrich, V., Pypaert, M., Mellman, I., Dembo, M., Mooseker, M.S., Wu, D., and Flavell, R.A. (2006). Modulation of cell adhesion and motility in the immune system by Myo1f. Science *314*, 136–139.

Krummel, M.F., Sjaastad, M.D., Wülfing, C., and Davis, M.M. (2000). Differential clustering of CD4 and CD3zeta during T cell recognition. Science *289*, 1349–1352.

Laakso, J.M., Lewis, J.H., Shuman, H., and Ostap, E.M. (2008). Myosin I can act as a molecular force sensor. Science *321*, 133–136.

Maravillas-Montero, J.L., Gillespie, P.G., Patiño-López, G., Shaw, S., and Santos-Argumedo, L. (2011). Myosin 1c participates in B cell cytoskeleton rearrangements, is recruited to the immunologic synapse, and contributes to antigen presentation. J. Immunol. *187*, 3053–3063.

McConnell, R.E., and Tyska, M.J. (2010). Leveraging the membrane - cytoskeleton interface with myosin-1. Trends Cell Biol. *20*, 418–426.

Mempel, T.R., Henrickson, S.E., and Von Andrian, U.H. (2004). T-cell priming by dendritic cells in lymph nodes occurs in three distinct phases. Nature *427*, 154–159.

Miller, M.J., Wei, S.H., Cahalan, M.D., and Parker, I. (2003). Autonomous T cell trafficking examined in vivo with intravital two-photon microscopy. Proc. Natl. Acad. Sci. USA *100*, 2604–2609.

Miramontes, O., Boyer, D., and Bartumeus, F. (2012). The effects of spatially heterogeneous prey distributions on detection patterns in foraging seabirds. PLoS ONE *7*, e34317.

Mrass, P., Petravic, J., Davenport, M.P., and Weninger, W. (2010). Cell-autonomous and environmental contributions to the interstitial migration of T cells. Semin. Immunopathol. *32*, 257–274.

Nambiar, R., McConnell, R.E., and Tyska, M.J. (2009). Control of cell membrane tension by myosin-I. Proc. Natl. Acad. Sci. USA *106*, 11972–11977.

Olety, B., Wälte, M., Honnert, U., Schillers, H., and Bähler, M. (2010). Myosin 1G (Myo1G) is a haematopoietic specific myosin that localises to the plasma membrane and regulates cell elasticity. FEBS Lett. *584*, 493–499.

Oster, G.F., and Perelson, A.S. (1987). The physics of cell motility. J. Cell Sci. Suppl. *8*, 35–54.

Overstreet, M.G., Gaylo, A., Angermann, B.R., Hughson, A., Hyun, Y.M., Lambert, K., Acharya, M., Billroth-Maclurg, A.C., Rosenberg, A.F., Topham, D.J., et al. (2013). Inflammation-induced interstitial migration of effector $CD4^+$ T cells is dependent on integrin αV. Nat. Immunol. *14*, 949–958.

Patino-Lopez, G., Aravind, L., Dong, X., Kruhlak, M.J., Ostap, E.M., and Shaw, S. (2010). Myosin 1G is an abundant class I myosin in lymphocytes whose localization at the plasma membrane depends on its ancient divergent pleckstrin homology (PH) domain (Myo1PH). J. Biol. Chem. *285*, 8675–8686.

Pope, C., Kim, S.K., Marzo, A., Masopust, D., Williams, K., Jiang, J., Shen, H., and Lefrançois, L. (2001). Organ-specific regulation of the CD8 T cell response to Listeria monocytogenes infection. J. Immunol. *166*, 3402–3409.

Preston, S.P., Waters, S.L., Jensen, O.E., Heaton, P.R., and Pritchard, D.I. (2006). T-cell motility in the early stages of the immune response modeled as a random walk amongst targets. Phys. Rev. E Stat. Nonlin. Soft Matter Phys. *74*, 011910.

Reynolds, A.M., and Bartumeus, F. (2009). Optimising the success of random destructive searches: Lévy walks can outperform ballistic motions. J. Theor. Biol. *260*, 98–103.

Serrador, J.M., Nieto, M., and Sánchez-Madrid, F. (1999). Cytoskeletal rearrangement during migration and activation of T lymphocytes. Trends Cell Biol. *9*, 228–233.

Textor, J., Peixoto, A., Henrickson, S.E., Sinn, M., von Andrian, U.H., and Westermann, J. (2011). Defining the quantitative limits of intravital two-photon lymphocyte tracking. Proc. Natl. Acad. Sci. USA *108*, 12401–12406.

Usherwood, E.J., Hogg, T.L., and Woodland, D.L. (1999). Enumeration of antigen-presenting cells in mice infected with Sendai virus. J. Immunol. *162*, 3350–3355.

Vicente-Manzanares, M., Sancho, D., Yáñez-Mó, M., and Sánchez-Madrid, F. (2002). The leukocyte cytoskeleton in cell migration and immune interactions. Int. Rev. Cytol. *216*, 233–289.

Woolf, E., Grigorova, I., Sagiv, A., Grabovsky, V., Feigelson, S.W., Shulman, Z., Hartmann, T., Sixt, M., Cyster, J.G., and Alon, R. (2007). Lymph node chemokines promote sustained T lymphocyte motility without triggering stable integrin adhesiveness in the absence of shear forces. Nat. Immunol. *8*, 1076–1085.

Wülfing, C., Rabinowitz, J.D., Beeson, C., Sjaastad, M.D., McConnell, H.M., and Davis, M.M. (1997). Kinetics and extent of T cell activation as measured with the calcium signal. J. Exp. Med. *185*, 1815–1825.

Zhdanov, V.P., Pavlicek, J., and Knor, Z. (1988). Preexponential factors for elementary surface processes. Catal. Rev. *30*, 501–517.